

Continuous thermal histories from closure profiles

T. Mark Harrison

*Research School of Earth Sciences
The Australian National University
Canberra, A.C.T. 0200, Australia*

Marty Grove, Oscar M. Lovera

*Department of Earth and Space Sciences
University of California, Los Angeles
Los Angeles, CA 90095, U.S.A.*

Peter K. Zeitler

*Department of Earth and Environmental Sciences
Lehigh University
Bethlehem PA 18015, U.S.A.*

INTRODUCTION

Background

Most geophysical processes impart a characteristic thermal signature to the crust that can be preserved in the form of isotopic variations in radiogenic minerals. Reading the record of these events using thermochronology permits unprecedented insights into the timing and rates of key dynamic processes, such as rifting, thrust faulting, tectonic denudation, erosion/incision, and magmatism, that may otherwise go unnoticed (McDougall and Harrison 1999). However, heat flow disturbances are often too subtle to be revealed by conventional thermochronometric methods; i.e., interpolation of temperature-time data from bulk analyses. Rather, the highest resolution thermal histories require harnessing knowledge of the concentration distribution of the daughter product in the mineral of interest.

In previous chapters, the case has been explored in which a mineral cooling within the crust transitions from being open to loss of daughter product to closed system behavior. Assuming a monotonic thermal history of simple form (Dodson 1973), it is then possible to use the balance between radiogenic accumulation and loss to assign a bulk closure temperature, T_c , given by:

$$\frac{E}{\Re T_c} = \ln \left(\frac{A \Re T_c^2 D_0 / r^2}{E dT/dt} \right) \quad (1)$$

where E is the activation energy, D_0 is the frequency factor, \Re is the gas constant, T is absolute temperature, A is a geometry factor (sphere = 55, cylinder = 27, and plane sheet = 8.7), r is the effective diffusion length scale, and dT/dt is cooling rate. When the T_c and age of a number of coexisting mineral thermochronometers are correlated, an estimate of the temperature history can be interpolated. This method, termed the bulk closure approach, has been used for over 25 years (Purdy and Jäger 1976; Mattinson 1977; Harrison et al. 1979; Berger et al. 1979).

However, use of Eqn. (1) carries several stringent requirements. These include: knowledge of the activation energy, frequency factor, and compositional dependence of daughter product diffusion in the mineral of interest, *a priori* knowledge of the effective diffusion dimension, and assurance that volume diffusion was the rate limiting natural transport mechanism. Although adequate diffusion data are available for most commonly used minerals, it is only in rare cases that all these requirements are met. This represents a significant limitation of thermochronometry.

An example: the bulk closure temperature of biotite

Consider the example of Ar closure in ‘biotite’, which is typically taken to be $300\pm 50^\circ\text{C}$ (Purdy and Jäger 1976; Mattinson 1978; Harrison et al. 1979; Hodges 1991). This represents a nearly ideal case as the biotite-phlogopite solid solution is experimentally well-characterized in terms of Ar diffusion (Giletti 1974; Giletti and Tullis 1977; Harrison et al. 1985; Grove and Harrison 1996). Nevertheless, rigorous determination of a closure temperature requires that we know: 1) the effective diffusion length scale, 2) important compositional parameters such as Fe/Mg ratio, Al (VI) occupancy, and halogen content, 3) the approximate cooling rate and pressure during Ar closure (see Harrison and Zeitler 2005). For example, a biotite with an Fe/Mg of 0.6, an Al(VI) occupancy of 1.0, a total halogen content of 0.2%, and $r = 150\ \mu\text{m}$, is characterized by a T_c of 350°C (assuming $P = 200\ \text{MPa}$ and $dT/dt = 100^\circ\text{C}/\text{Ma}$). However, increasing the total halogen content to 0.8% and decreasing Fe/Mg to 0.4 increases T_c to about 450°C (Grove 1993). Together with published estimates of r that vary by a factor of 6, extreme variations in compositional parameters yield a range in ‘biotite’ T_c of over 300°C .

The magnitude of this range would be of less concern if it could be reported that the compositional and diffusion size parameters were routinely measured. However, to our knowledge, only a handful of the many hundreds of studies involving Ar closure in biotite have actually attempted to do so (e.g., Harrison et al. 1985; Copeland et al. 1987).

Bulk mineral thermochronometry

Implicit in the example just discussed is that the underlying assumptions of the closure temperature model have been met (i.e., $\tau = \mathcal{R}T_c^2/E \cdot dT/d \gg r^2/D(0)$, linear cooling in $1/T$, no inherited daughter, no subsequent open system behavior, no recrystallization; see Harrison and Zeitler (2005) for definitions). If so, then the bulk T_c calculated for the biotite can be combined with the measured K-Ar age to yield a temperature-time ($T-t$) datum on a thermal history plot. Figure 1(a) shows a schematic $T-t$ plot with three mineral thermochronometers of contrasting closure temperature. As an example, the input thermal history (solid curve) shown is meant to represent initially slow cooling in the mid-crust, followed by rapid cooling in the footwall of a rapidly slipping normal fault, and then slow cooling due to erosional denudation.

In such a case, it is possible to use the transition from slow to rapid cooling to determine both the initiation age of faulting and the slip rate by fitting the form of the thermal history to an appropriate thermo-kinematic model (Harrison et al. 1995, 1996). Note, however, that the resolution of the bulk closure data set is insufficient to reveal the complex nature of the temperature evolution (Fig. 1a). Indeed, there is no justification to infer anything other than the linear history, shown by the dashed line, which misses the essential character of the $T-t$ path.

How do we obtain the highest accuracy and resolution thermal histories?

We have, thus far, emphasized that bulk closure temperatures are only rarely rigorously determined and that temperature-time histories generated from such data are characterized by relatively low resolution. These limitations can be appreciated by inspection of Eqn. (1). Because T_c varies as the natural logarithm of a term that typically has a value in the range of 10^{16} - 10^{18} , it is highly insensitive to variations in the constituent parameters, including dT/dt . It stands to reason that inverting the problem to solve for time-dependent variations in dT/dt would yield far greater sensitivity, provided T_c could be precisely determined. In fact, Dodson (1973) did just that. The full accumulation-diffusion-cooling equation for a time-dependent diffusion coefficient was solved to yield expressions for the distribution of the daughter product within solids of various geometries. When volume averaged, they reduce to the form given by Eqn. (1).

In cases where thermal variations are too subtle to be revealed by the interpolation method, they may be documented by harnessing the full concentration distribution equation. This general approach is shown schematically in Figure 1(b) where knowledge of the daughter product distribution has permitted determination of a continuous thermal history of complex form. The bounding envelope represents an objective estimate of the range of uncertainty associated with the T - t path.

IN SITU CLOSURE PROFILES

The closure profile equation

To restate the preceding paragraph, although a mineral can be characterized by a bulk T_c , each radial position within the crystal has a unique closure temperature, the volume average of which is the parameter described by Eqn. (1). Dodson (1973) presented, but did not evaluate, expressions for the limiting concentration distributions within minerals following slow cooling. Dodson (1986) later obtained solutions for the distribution of daughter/parent as a function of position within a cooling solid for sphere, cylinder and plane sheet geometries. The closure profile equation is given by:

$$\frac{E}{\Re T_c} = \ln(\gamma \tau D_0 / r^2) + 4S_2(x) \quad (2)$$

where $\gamma = 1.78$, $\tau = \Re T_c^2 / E \cdot dT/dt$, and $4S_2(x)$ describes the concentration distribution for different geometric solutions. Summations of $4S_2(x)$ (Dodson 1986) as a function of position within plane sheet, spherical, and cylindrical solids are given in Table 1. Note that when the volume averaged value of $4S_2(x)$ (Table 1) is inserted into Eqn. (2), it reverts to the form of Eqn. (1).

Because the boundary concentration is maintained at zero (i.e., it is always open), the closure temperature tends to zero as the boundaries are approached (i.e., $x \rightarrow \pm 1$). The broader implication of Eqn. (2) is that a single mineral sample can provide a continuous cooling curve rather than only a single temperature–time point.

INFERRING CLOSURE PROFILES FROM $^{40}\text{Ar}/^{39}\text{Ar}$ DATA

The $^{40}\text{Ar}/^{39}\text{Ar}$ method is among the most versatile thermochronologic tools (McDougall and Harrison 1999; see also Harrison and Zeitler 2005). It offers both the potential of constraining continuous thermal histories by direct determination of *in situ* age profiles and indirect analysis based upon step-heating of bulk materials. The indirect nature of the step-heating approach stems from the fact that the age distribution is deduced from measurement of the relative flux of ^{40}Ar and ^{39}Ar from all portions of the bulk material as a function of temperature (see Harrison and Zeitler 2005).

Direct measurement of $^{40}\text{Ar}/^{39}\text{Ar}$ age profiles in single crystals is a promising approach that is primarily limited by analytical difficulties. Consider the case of a biotite ($\text{Fe}/\text{Mg} = 0.6$, $E = 47$ kcal/mol, $D_0/r^2 = 350/\text{s}$; Harrison et al. 1985) that cooled at $5^\circ\text{C}/\text{Ma}$ through the Ar closure interval, which equates to a bulk closure temperature of 300°C (infinite cylinder geometry). The radial distribution of closure temperature using Eqn. (2) varies from 325°C at $x = 0$ to 240°C at $x = 0.99$, in accord with our expectation of a high T_c in the center and a lower T_c near the diffusion boundary. Thus if the spatially varying age distribution is known, we can in theory determine the variation of τ , which is directly related to dT/dt , as a function of time.

A significant amount of effort has gone into laser probe analysis of millimeter-scale single crystals of mica and other phases (Lee et al. 1990; Onstott et al. 1991; Scaillet et al. 1991; Hodges et al. 1994; Arnaud and Kelly 1995; Reddy et al. 1996; Pickles et al. 1997). Results from these studies have demonstrated that application of laser ablation is capable of revealing significant age variation in mm-scale crystals and could, under favorable circumstances, lead to thermal history constraints (Hodges et al. 1994; Hames and Andresen 1996; Hames and Cheney 1997; Kelly and Wartho 2000; Wartho and Kelley 2003). Alternatively, *in situ* laser analysis has proven exceedingly useful for revealing problematic excess ^{40}Ar distributions. Some of the best examples occur in phengitic micas from relatively dry, ultra high-pressure rocks (Kelly et al. 1994; Arnaud and Kelley 1995; Sherlock et al. 1999).

In spite of its potential, the major limitation for *in situ* laser age profiling of grains remains the fact that some (not all) intracrystalline features that control Ar transport in $^{40}\text{Ar}/^{39}\text{Ar}$ thermochronometers appear to be very small (i.e., $< 1 \mu\text{m}$; e.g., Foland 1974) relative to the dimensions of ablation pits that liberate sufficient argon to accurately resolve age variation ($\sim 10 \mu\text{m}$ for >1 Ga materials and much larger for more youthful minerals). Thus even though depth profiling approaches have been developed to enhance spatial resolution in close proximity to grain boundaries (e.g., Arnaud and Kelly 1997; Wartho et al. 1999), key information remains out of reach for spot profiling approaches that lack the spatial resolution to detect $< 10 \mu\text{m}$ scale features. Because of this limitation, the most significant developments have come in the realm of interpreting age spectra obtained from bulk step-heating of anhydrous materials that remain stable over a broad range of conditions during *in vacuo* heating (e.g., Lovera et al. 1993). Such experiments are sensitive to all length scales larger than those characteristic of ^{39}Ar recoil ($\sim 0.1 \mu\text{m}$) and are capable of simultaneously revealing both the age and kinetic properties of Ar in the thermochronometer.

$^{40}\text{Ar}/^{39}\text{Ar}$ step-heating of K-feldspar

By far the best opportunity to obtain detailed thermal histories from the K-Ar system is by application of $^{40}\text{Ar}/^{39}\text{Ar}$ step-heating method to K-feldspars. K-feldspar is ideal in this role as it is widespread, ^{40}K rich, and generally stable during laboratory heating up to temperatures near its melting point ($\sim 1100^\circ\text{C}$). Two distinct sources of information are available from a K-feldspar $^{40}\text{Ar}/^{39}\text{Ar}$ step-heating experiment: the age spectrum (Fig. 2a) and the Arrhenius plot (Fig. 2b). The age spectrum is calculated from the flux of radiogenic argon ($^{40}\text{Ar}^*$) relative to the reactor produced argon ($^{39}\text{Ar}_K$) that is released during discrete laboratory heating steps (see Harrison and Zeitler 2005). The Arrhenius plot is derived by plotting diffusion coefficients (calculated from inversion of the ^{39}Ar release function assuming a single diffusion length scale) against the inverse absolute

temperature of laboratory heating. Because the shape of the Arrhenius plot varies with laboratory heating schedule for samples containing a distribution of domain sizes, an alternate form of data display termed the $\log (r/r_o)$ plot is often used (Richter et al. 1991; Fig. 2a). $\log (r/r_o)$ spectra are constructed by plotting the deviation of the measured diffusivities (D/r^2) from a reference diffusion law ($D/r_o^2 = D_o/r_o^2 \cdot \exp[E/\mathcal{R}T]$) at a given temperature T as a function of cumulative % ^{39}Ar released (Fig. 2b). Because the intrinsic diffusivity D from the reference diffusion law is arbitrarily assigned to the sample, the $\log (r/r_o)$ value is given simply by the expression $0.5 \cdot (\log D/r_o^2 - \log D/r^2)$.

Without exception, $^{40}\text{Ar}/^{39}\text{Ar}$ age spectra of basement K-feldspars yield age spectra and Arrhenius plots that are inconsistent with the presence of a single diffusion dimension. For example, rather than yielding a single linear array, K-feldspar Arrhenius plots show complex departures from an initial straight line segment (e.g., Fig. 2b). These behaviours undoubtedly reflect discrete Ar retentivities within K-feldspar, whether due to varying size, energetics, nested diffusion domains, or other phenomena.

Fundamental assumptions for recovering thermal history information

Two fundamental assumptions that must be satisfied to permit estimation of crustal thermal histories from K-feldspar $^{40}\text{Ar}/^{39}\text{Ar}$ step-heating data. These include: (1) both $^{40}\text{Ar}^*$ and $^{39}\text{Ar}_K$ loss from K-feldspar is governed by volume diffusion; (2) laboratory Ar release adequately mimics the natural diffusion boundaries and mechanisms. Failure of either of these assumptions precludes recovery of useful thermal history data. By comparison, other commonly made assumptions are second order conditions (i.e., uniform $^{39}\text{Ar}_K$ distribution, regular diffusion geometry (slab, cylinder, sphere), zero $^{40}\text{Ar}^*$ boundary conditions, etc.) that can be dealt with by appropriately adjusting interpretative models. The reader may be aware that there is continued discussion of the relative importance of these and other factors in controlling Ar diffusion in K-feldspars (e.g., Parsons et al. 1999; Lovera et al. 2002). However, it is a truism that the *only* fundamental requirement for recovering thermal histories from $^{40}\text{Ar}/^{39}\text{Ar}$ step-heating results is knowledge that Ar loss proceeds by volume diffusion and that laboratory Ar release adequately mimics the natural diffusion boundaries and mechanisms.

Evaluation of Fundamental Assumptions. Examination of the similarity of the age and $\log (r/r_o)$ spectra yielded by a K-feldspar provides a first order assessment of the degree to which fundamental assumptions have been upheld. The age spectrum reflects the natural Ar retentivity of the sample over 10's of millions of years of cooling, whereas the Arrhenius data from which the $\log (r/r_o)$ plot was developed was generated on timescales of minutes to days. When $^{40}\text{Ar}^*$ concentration along diffusion boundaries are negligible, simple volume diffusion theory predicts that age spectra should increase monotonically with progressive ^{39}Ar release because natural $^{40}\text{Ar}^*$ concentrations should be highest in the most retentive sites. Exhibition of this predicted behavior represents the initial criterion for selecting samples for thermal history analysis.

The useful (i.e., most readily interpreted) fraction of gas release in a K-feldspar $^{40}\text{Ar}/^{39}\text{Ar}$ step-heating experiment is invariably limited at low-temperature by weakly bound (fluid inclusion-hosted?) excess radiogenic ^{40}Ar ($^{40}\text{Ar}_E$) and at high-temperature by the onset of melting (Fig. 2a). Within this interval, we often see correlated behavior between K-feldspar age and $\log (r/r_o)$ spectra. Correlated behavior is expected only if Ar diffusion occurs by the same mechanisms and has access to the same diffusion boundaries in nature as it does in the laboratory heating. In the case of N13 K-feldspar in

Figure 2, the age and $\log(r/r_0)$ spectra show correlated inflections at ~15%, 25%, and 50% ^{39}Ar released (Fig. 2a). We regard this as confirming evidence that, for this sample, diffusion properties obtained via step-heating experiments can be extrapolated to conditions attending natural Ar loss within the crust.

Lovera et al. (2002) developed routines to quantitatively evaluate the extent of correlation between age and $\log(r/r_0)$ spectra. About two-thirds of K-feldspars they analyzed gave correlation coefficients >0.9 and thus are well-suited for thermal history analysis. N13 K-feldspar, the example in Figure 2, yielded a correlation coefficient of 0.98. While some K-feldspars yield low (<0.9) correlation coefficients, this is generally due to contamination by excess Ar or presence of intermediate age maxima (see below). In contrast, hydrous phases (hornblende, biotite, muscovite) characteristically yield poorly – or even negatively – correlated age and $\log(r/r_0)$ spectra (Lovera et al. 2002).

Recognition of problematic behavior in K-feldspar $^{40}\text{Ar}/^{39}\text{Ar}$ age spectra

High Temperature $^{40}\text{Ar}_E$ Contamination. While most samples are adversely affected by at least some low-temperature $^{40}\text{Ar}_E$ at low temperatures (Fig. 2a), its existence is generally not a fatal problem since it is readily identified and can often be corrected for if step-heating experiments are designed appropriately (e.g., Harrison et al. 1994). When this is done, systematically varying age spectra similar to those shown in Figure 3a are often obtained when samples represent varying positions relative to a major structure such as a fault. Geologically significant age variation can be obscured however, when the high-temperature $^{40}\text{Ar}_E$ contamination is pervasive, as shown in Figure 3b. In general, such samples will be highly unfavorable candidates for thermochronology since reliable correction schemes are unknown.

The hallmark of $^{40}\text{Ar}_E$ contamination is highly erratic $^{40}\text{Ar}^*$ release (Fig. 3b). This generally has a large negative impact upon the degree of correlation between age and $\log(r/r_0)$ spectra (Foster et al. 2001). Characteristic “U-shaped” spectrum are typically obtained (e.g., Zeitler and Fitzgerald 1986). Independent geologic constraints often indicate that the least affected, and hence geologically most meaningful portion of the age spectrum occurs after low-temperature $^{40}\text{Ar}_E$ has been exhausted (by about ~600-800°C in typical step-heating sequences) and release of high-temperature $^{40}\text{Ar}_E$ is still minimal. This comparatively unaffected portion of gas release typically occurs at about 15-35 cumulative % $^{39}\text{Ar}_K$ release in relatively high resolution step-heating experiments. Release of high-temperature $^{40}\text{Ar}_E$ generally begins in earnest above ~900-1000°C or at temperatures that approach those required for melting K-feldspar *in vacuo*. The onset of $^{40}\text{Ar}_E$ is often easily recognized by rapidly increasing and highly erratic apparent ages that can exceed maximum ages permitted by independent geologic constraints. For such samples, it is only possible to interpret the lower temperature gas release provided that adequate corrections for low-temperature $^{40}\text{Ar}_E$ can be performed.

Intermediate age maxima (IAM). Intermediate age maxima are readily distinguished from the effects of $^{40}\text{Ar}_E$ in that they are typically expressed by smoothly varying “humps” over the portion of age spectrum where $^{40}\text{Ar}_E$ contamination is minimal (Fig. 3c). Such features are characteristic of K-feldspars that have experienced low-temperature alteration by authigenic adularia (Girard 1991; Foland 1994; Warnock 1999). While the underlying causes of IAM are not specifically known, they can potentially be explained by recrystallization, exsolution or other related phenomenon that has occurred at sufficiently low-temperatures to remobilize previously “locked in” $^{40}\text{Ar}^*$ that had

resided within the most retentive crystalline domains that are expected to yield the oldest ages. We will revisit the implications of such misbehavior once we have introduced the multi-diffusion domain model and the techniques employed to recover thermal history information from K-feldspar.

To summarize, $^{40}\text{Ar}_E$ contamination generally appears to reflect incorporation of radiogenic argon from external sources that is either loosely bound (i.e., within fluid inclusions) or tightly held (potentially in higher order defects or similar features in crystalline K-feldspar). Alternatively, existence of IAM appears likely reflects problematic redistribution of intrinsic $^{40}\text{Ar}^*$ (i.e., derived from *in situ* radiogenic decay of ^{40}K) from high retentivity to low retentivity domains in K-feldspar. Finally, although Figure 3d implies that these types of misbehavior are manifested in the minority of K-feldspars that we have examined, samples that have experienced similar histories will tend to exhibit similar age spectra. *In other words, in settings where problematic behavior is manifested, it will tend to be prevalent.*

The multi-diffusion domain model

The multi-diffusion domain (MDD) model (Lovera et al. 1989, 1991) assumes that the characteristic form of the Arrhenius plot and age spectrum in K-feldspars is due to the presence of a discrete distribution of diffusion domain sizes. Thus the form of both plots is a function of the diffusion (E and D_0) and domain distribution (domain size, ρ , and volume fraction, ϕ) parameters and the form of the thermal history. The sample Arrhenius plot is a convolution of the parameters that characterize the individual diffusion domains. Since the diffusion parameters are obtained directly from the Arrhenius plot and we have two independent measures of ρ and ϕ (i.e., the $\log(r/r_0)$ plot and age spectrum), in theory we have sufficient information to invert the results to obtain a unique, monotonic cooling history.

As noted earlier, there is a diversity of opinion regarding the cause of discrete Ar retentivities in K-feldspar, with some workers disputing the role of diffusion domain size as the primary cause. In fact, a faithful depiction of the intrinsic structure of K-feldspar is not required to calculate a meaningful thermal history. Any diffusion-based model, for example one in which nested diffusion domains interact (e.g., the heterogeneous diffusion model; Lovera et al. 2002) will accurately reproduce the same thermal history as predicted by the MDD model provided the conservation of diffusion mechanism and boundary assumptions are met.

Thermal history calculations based upon the MDD model begin by estimating the diffusion parameters E and $\log(D_0/r_0^2)$ for the K-feldspar in question. This may be accomplished by least squares fitting to the linear initial low-temperature Arrhenius data (Lovera et al. 1997) (Fig. 4a). The slope defined by this low-temperature data is expected to be proportional to $-E/\mathfrak{R}$ provided that none of the domains contributing ^{39}Ar have been outgassed by more than ~60% (Lovera et al. 1991). It is also possible to employ average values for (~46 kcal/mol; see Lovera et al. 1997) when the initial gas release fails to adequately define E and $\log(D_0/r_0^2)$. The next step is to find a set of distribution parameters, volume fraction (ϕ) and the relative size (ρ) for each domain, that best fit the measured Arrhenius data. The domain distribution for N13 K-feldspar is indicated schematically on Figure 4a. Once the MDD diffusion model has been calibrated for the K-feldspar in question, it is possible to perform forward modeling by iteratively inputting trial thermal histories (Fig. 4b) to calculate model age spectra (Fig. 4c). Note that initial

temperatures must be high enough to exceed the closure temperatures of the largest domains (i.e., $\gg 400^\circ\text{C}$).

To be sure, one can do very well using the equations of Lovera et al. (1989) to conduct forward modelling, using experience to be fairly efficient at finding a solution. However, this can become tedious with larger numbers of samples, and leaves open the nagging concern that even when applying available geologic constraints that the one solution arrived at is only one of a number of possibilities. Intuitively, given the good precision of most $^{40}\text{Ar}/^{39}\text{Ar}$ measurements and some experience with forward modelling, one expects that for most cases of simple monotonic cooling, K-feldspar age spectra provide tight constraints on thermal history, and experiments with the inverse models described below bear this out. However, given that it appears that most multidomain samples can be described using a single activation energy, the time-temperature response of different domains will be similar. Thus in the case of more complicated thermal histories involving thermal stagnation or reheating, the range of possible solutions will be larger and quite possibly disparate.

Inversion of $^{40}\text{Ar}/^{39}\text{Ar}$ to thermal history data

Calculating continuous thermal histories directly from measured closure profile entails relatively straightforward and direct inversion using the closure-profile equation. Observation of the distribution of ^{40}Ar in K-feldspars is more complicated, owing to the diffusion-domain structure prevalent in feldspars, and the indirect method used in assessing this distribution via measurements of ^{40}Ar and ^{39}Ar fluxes via diffusion during step-heating. In a manner analogous to the way in which information about the Earth's interior structure is obtained – using observed seismic data to invert for velocity structure or other parameters, and thus obtain tomographic images of the Earth's interior that can be interpreted in terms of temperature or rheology – we wish to find the set of all temperature histories that can explain our observed data, which take the form of a flux ratio of $^{40}\text{Ar}/^{39}\text{Ar}$ and the absolute quantity of ^{39}Ar degassed from K-feldspar diffusion boundaries.

In general, inversion of age spectra is no more or less complicated than inversion of other data sets. One's goal is to minimize an objective function which amounts to the difference between observed and predicted values. This in practice involves code which can be used to calculate predicted values from parameters (i.e., a forward model) and then some recipe for manipulating parameters so that they are progressively shaped to minimize the value of the objective function. Different schemes have their advantages and disadvantages in terms of overall efficiency, speed towards a solution, and predilection for becoming trapped in a false minimum. For instance, a purely Monte Carlo approach is quite simple to implement, generally good at exploring parameter space without becoming trapped, but impossibly inefficient for use with thermochronological data, given the range of thermal histories to explore and the temperature sensitivity of diffusion. Basic simplex methods (see Press et al. 1998) are fairly efficient but can quite readily crawl into a false minimum and become happily trapped. Below, we describe two approaches that seem to do quite well in balancing efficiency with adequate investigation of parameter space.

Controlled random search method. For the purpose of inverting apatite fission-track data for thermal history, Willet (1997) described an implementation of the controlled random search algorithm of Price (1977). This algorithm retains the

advantages of a Monte Carlo approach in searching parameter space for true minima, while converging far more rapidly due to the “learning” component inherent in the CRS method. Zeitler (1993, 2004) adapted Willet’s approach for use with K-feldspar age spectra under the assumptions of the multidomain model described above, most recently adding the ability to include other thermochronometers in the inversion process.

As applied to thermochronological data, the CRS algorithm manipulates a starting pool of ~150 randomly generated thermal histories, generating a new history from a subset of some ~10 histories randomly chosen from the master pool, testing it and accepting it into the pool if it provides a better fit between the observed and calculated age spectra (and other ages). In detail, the new history is made as follows: the histories in the subset are averaged, and then the new history is made by reflecting the additional selected history through the averaged values, subject to an amplification factor that might range between 1.1 and 1.5. Thus, as the master pool of histories learns about better solutions and is improved, new histories inherit something of this learning, although incompletely, since they are made from only a small subset. In addition, the reflection and amplification process serves to introduce diversity into the pool and together these two factors serve to explore parameter space while helping the model avoid traps in the form of false minima.

The code which implements the CRS algorithm, Arvert, uses at its core the equations of Lovera et al. (1989) to calculate K-feldspar age spectra from thermal histories, and uses a finite-difference scheme to model results from other systems like U-Th/He. The fit between observed and calculated data can be assessed using either a simple mean percent deviation determined from all relevant steps and other mineral ages, or using a chi-square parameter that takes into account uncertainties on the observed data. The user has the option of providing both explicit constraints in the form of temperature boundaries at various times in the model run, as well as implicit rate constraints for maximum heating and cooling rates.

Figure 5 shows a typical Arvert convergence sequence for synthetic data, determined for linear cooling of a multidomain sample at 10°C/m.y. For these synthetic data, the convergence criterion was arbitrarily chosen at a mean percent deviation of one percent. It is clear from the convergence sequence that the model very quickly learns about impossible portions of parameter space (old and cold, young and hot), and then begins to hone in on the correct cooling rate over that portion of temperature-time space where the age spectrum has constraining power. Figure 6 shows that the model has little trouble recovering more complex, non-linear cooling histories, and that addition of other mineral data into the inversion, such as low-temperature U-Th/He apatite data, can significantly extend and improve the quality of the results.

Beyond the intrinsic value and convenience of having an automated, objective means of assessing K-feldspar age spectra and the thermal histories that might be compatible with them, use of such models brings into focus several technical details that can be overlooked. One is the great importance of adequately and accurately determining a sample’s domain structure; “extra” domains do no harm but working with an insufficient number of domains that do not truly represent the domain distribution lead to poor fits and poor convergence, because, obviously, one is in effect violating the fundamental assumption that the geologic and laboratory diffusion experiments are happening in the same structure. A second item to keep in mind is that the 150°C or more

of thermal history that can be recorded by a K-feldspar is not in most cases uniformly distributed along the length of an age spectrum: the smaller domains usually have a lesser volume fraction but record a significant part of the lower-temperature thermal history. It is this part of the history that is most often obscured by excess or Cl-correlated trapped Ar, and most often ignored by beginners as they focus on an overall age-spectrum fit, and in fact can be the last portion of an age spectrum that the inversion code improves. Care is needed with dealing with initial parts of an age spectrum, and this is an added motivation for including other low-temperature thermochronometers in the inversion to provide additional constraints.

The variational approach. An alternative method utilized by Lovera et al. (1997) to fit both the Arrhenius and age data is the Levenberg-Marquardt variational approach (Press et al. 1988). The determination of the domain distribution parameters, (ρ, ϕ) , involves the fitting of the cumulative ^{39}Ar released from the step heating experiment. The Levenberg-Marquardt scheme has proven proficient in searching the parameter space (ρ, ϕ) for the set of values that produced the best fit to the measured ^{39}Ar data (Lovera et al. 1997). While the domain distribution (ρ, ϕ) that produced the “best-fit” solution is non-unique, all potential solutions tend to produce equivalent effects that are minor when compared to the impact of varying activation energy (Lovera et al. 1997). Because of the impact that E has upon thermal history calculations, Lovera et al. (1997) found it desirable to perform calculations in a manner in which this parameter is explicitly varied. To accomplish this, a number of equivalent domain distributions are determined by randomly selecting values of E and $\log D_0/r_0^2$ from a normal distribution centered upon the measured values (see Lovera et al. (1997) for details).

A similar Levenberg-Marquardt method can also be employed to model the $^{40}\text{Ar}/^{39}\text{Ar}$ age spectrum. Since the diffusion and domain distributions are constrained by the ^{39}Ar release data, the only degree of freedom in modeling the age spectrum is given by the thermal history. Thus, a parametric expression for the thermal history must be specified. One approach is to employ a Chebyshev polynomial function to represent the thermal history. The phase of this expansion can be conveniently varied to iterate from a random initial history towards solutions that fits the observed age spectrum to a specified degree. For each set of MDD parameters, a number of best-fit thermal history solutions to the measured age spectrum are then sought beginning with initial, random thermal histories. In practice, calculating 10 equivalent domain distributions and seeking five best-fit solutions to the age spectrum for each (50 total best-fit solutions) appears to adequately explore the impact of varying E .

Results obtained by applying this approach to 96MX-001 K-feldspar are shown in Figure 7. Correction of the low-temperature steps for Cl-correlated $^{40}\text{Ar}_E$ allowed us to fit the age spectrum between 10 and 58 Ma (Fig. 7a). The corresponding cooling histories reflect propagation of a ± 2 kcal uncertainty in E . This translated into a $\pm 17^\circ\text{C}$ temperature uncertainty (Fig. 7b). The 90% confidence limits of the mean and median of the resulting distribution of cooling histories are shown in Figure 7c. Note that the median confidence bands are limited to the portion of the thermal history that was constrained by age data from the K-feldspar. The Late Eocene-Early Oligocene rapid-cooling indicated by this sample corresponds with localized basement denudation that diverted extraregional drainages that had developed across the erosionally beveled terrane in the Eocene (Axen et al. 2000). Low-temperature constraints from K-feldspar constrain

the timing and magnitude of Late Miocene and Pliocene extensional faulting. Note that Paleocene rapid-cooling is not constrained by age data from the sample and is simply an artifact of the starting conditions.

Figure 8 compares the variational results for sample MX-100 with those obtained using the CRS approach. As indicated, both models yield very similar thermal histories for this sample in spite of using significantly different computational approaches and trial input thermal histories (compare Fig. 8c and 8d).

Numerical Simulation of Domain Instability during Slow-Cooling

All in all, inversion is not a panacea and is no substitute for careful assessment of data and understanding of multi-domain systematics. Users must be ever vigilant in assessing potentially problematic behavior. While samples affected by significant $^{40}\text{Ar}_E$ contamination are generally easily identified and avoided, samples exhibiting IAM often present a more subtle and hence insidious problem. As previously stated, IAM appear to reflect problematic redistribution of $^{40}\text{Ar}^*$ from larger domains to smaller domains. To quantify the effects of instantaneous domain reorganization during slow cooling, Lovera et al. (2002) performed numerical simulations based upon a finite difference algorithm based on the Crank-Nicholson implicit method (Crank 1975) to simulate diffusion through plane slabs with zero boundary conditions. A subset of their calculations is presented here. At a specified temperature, Lovera et al. (2002) instantaneously formed small domains that inherited Ar concentrations from their larger predecessors. In order to simplify interpretation, the sample was assumed to undergo linear slow-cooling and the initial and final domain distributions were characterized by the same set of diffusion length scales. Repartitioning of the domains in the eight domain sample was accomplished by readjusting the volume concentrations of the individual length scales. At a given temperature, a portion of the population of the smallest four domains was created at the expense of the four largest domains. The smallest domains inherited a uniform distributed concentration equivalent to the mean $^{40}\text{Ar}^*$ concentration that had been accumulated within the largest domains until that time. Because parent domains were 20-50 times larger than daughter domains, use of uniform $^{40}\text{Ar}^*$ concentrations within the newly created domains was justified.

In the most extreme domain transformation examined by Lovera et al. (2002), the proportion of the very smallest domains was increased at the expense of the very largest domains. Thirty-two percent of the bulk K-feldspar was affected. Calculated age spectrum resulting from transformation of the domain structure at four different temperatures (150, 200, 250, and 300°C) of the imposed linear cooling history are shown in Figure 9. As shown, the age spectrum remains unaffected when breakage occurs at or above 250°C. This is because even when the four smallest domains comprise more than 60% of the sample, they are completely open to Ar loss at that temperature. In such a case, MDD analysis produces an accurate estimate of the imposed thermal history. This is not the case for the 200°C and 150°C transformations however. An IAM that is just barely developed at 200°C becomes prominently developed for the 150°C solution (Fig. 9a). Concomitantly, the calculated thermal histories become increasingly nonsensical (Fig. 9b). It should be noted that it became impossible to obtain good MDD fits to the 200 and 150°C model age spectra.

Less extreme domain transformations considered by Lovera et al. (2002) produced more subtle effects whose impact was further decreased as the fraction of the bulk

feldspar involved was reduced. In spite of this, it was clear that significant restructuring of the domain structure under $<250^{\circ}\text{C}$ is capable of producing problematic artifacts in calculated thermal histories. Hence, extreme caution should be exerted in analyzing results from K-feldspars that have been either cataclastically deformed or partially altered to adularia under low-temperature ($<250^{\circ}\text{C}$) conditions.

Other Applications: Th-Pb dating of monazite

Background. Since the development of U-Pb ion microprobe dating 20 years ago, (Compston et al. 1984), the general approach has been to focus a primary beam of oxygen ions on a polished surface and analyze the secondary ions of Pb, U, and UO emitted. By comparison of Pb^+/U^+ vs. UO^+/U^+ of the unknown with a standard of known age, it is possible to date accessory minerals in this way with $\pm 1\%$ accuracy. The spatial resolution of such a measurement is defined by the diameter of the primary ion beam spot. Given the trace concentration levels of Pb usually encountered, typical ion probe spot diameters of 10-30 μm are generally required.

However, because virtually all secondary ions originate from the first or second atomic layer of the instantaneous sample surface, atomic mixing due to the impacting primary ions and geometric effects on crater production are the essential limiting factors on depth resolution. Provided the crystal contains symmetrical overgrowths, it is possible to use the ion microprobe in depth profiling mode on an unpolished surface to increase spatial resolution by up to two orders of magnitude relative to spot analysis. Care must be taken in this analysis mode to ensure material sputtered from the crater walls is not analyzed, typically by placing an aperture in front of the emergent ion beam that restricts entry into the mass spectrometer to only those ions originating on the crater floor. Once the sputtered crater shape and depth have been determined, usually using a surface profilometer, a continuous age profile as a function of depth is obtained. This works routinely in cases where the age profile is revealed over distances on the order of a few microns – the depth over which inter-element calibrations are stable. For deeper profiles, the sample can be re-polished after initial sputtering and the depth of the residual pit measured by surface profilometry to accurately calculate the thickness of sample removed. This approach has been applied to zircon and monazite (Mojzsis and Harrison 2002; Grove and Harrison 1999).

In cases where observed Pb loss can be attributed to volume diffusion, such gradients contain potentially valuable thermochronological information that can be extracted if the diffusion behavior of Pb were known with confidence.

Pb Diffusion in Monazite. Pb diffusion in monazite has been measured by Smith and Giletti (1997) and Cherniak et al. (2004), who obtained strikingly different results. Smith and Giletti (1997) measured the tracer diffusion of Pb under hydrothermal conditions in natural monazites using ion microprobe depth profiling and obtained an activation energy of 180 kJ/mol. Cherniak et al. (2004) measured Pb diffusion in synthetic and natural monazites under dry, 1-atm conditions using both Rutherford Backscattering Spectroscopy and ion microprobe depth-profiling methods. Their activation energy of 590 kJ/mol is more than three times higher than that reported by Smith and Giletti (1997). Although the source of this discrepancy remains unclear, it is generally accepted that the lowest value of diffusion coefficient measured is the best estimate as diffusion is the rate limiting transport mechanism in solids (i.e., any non-diffusive effect would increase D). While this would seem to favor the Cherniak et al.

(2004) study, they noted that linear extrapolation of their diffusion law for Pb in monazite to geologic conditions would preclude the existence of μm -scale profiles as seen in Figure 2a. They allowed that there might be a change in diffusion mechanism between the conditions attainable in the laboratory and that in nature and used the Grove and Harrison (1999) datum to estimate an activation energy of 345 kJ/mol. Although containing an element of circularity, we use this value of E in the subsequent discussion for the purposes of illustrating the approach.

Th-Pb age profile of monazite DH-68-96. Gneisses of the crystalline nappe that form the hanging wall of the Himalayan Main Central Thrust experienced Miocene peak metamorphic temperatures of 600 to 750°C, but cooled below ca. 400°C by 3 Ma (Harrison et al. 1999). Th-Pb depth profiling of monazites from sample DH-68-96, obtained from a 13 Ma pegmatite, revealed an age gradient within 1 μm of the crystal surface (Grove and Harrison 1999) (Fig. 10a). Secondary ion intensities were sufficient to permit $\sim 500\text{\AA}$ depth resolution. The continuous nature of these profiles, the relative conformity of their shape to that expected for radiogenic ingrowth/diffusion loss (Eqn. 2), and their inter-grain consistency effectively rules out protracted growth as an explanation for their formation. Thus it was concluded that the age gradient shown in Figure 2(a) is a closure profile. Given knowledge of Pb diffusion in monazite, the closure profile could then be used to extract a continuous thermal history using Eqn. (2).

Continuous thermal history. Given a diffusion law for Pb in monazite, albeit a problematic one, it remains only to fit the closure profile (Fig. 10a) using Eqn. (2). Repeated forward modeling to fit the age profile (Fig. 2a) leads to the thermal history shown in Figure 10b, which is characterized by initial rapid cooling to about 750°C followed by cooling at $\sim 20^\circ\text{C}/\text{m.y.}$ until 4 Ma when a second phase of rapid cooling begins. This history is consistent with thermometric data from the encompassing metamorphic rocks and the age of the coexisting biotite. Furthermore, the form of the thermal history (Pliocene rapid cooling in the MCT hanging wall) was predicted based on the pattern of recrystallization ages in the MCT footwall (Harrison et al. 1998).

CONCLUSION

The conventional approach to thermochronology, the bulk closure method, is limited by a set of underlying requirements that are rarely met. Obtaining the highest possible resolution thermal histories requires resolving spatially varying, intra-grain concentration distributions of the daughter product. At present, $^{40}\text{Ar}/^{39}\text{Ar}$ step-heating of K-feldspar represents the best opportunity to recover continuous thermal history information. Other methods, such as Th-Pb depth profiling of monazite, are highly promising but require resolution Pb diffusion laws for monazite.

K-feldspar provides an extraordinary opportunity to obtain continuous thermal histories by application of $^{40}\text{Ar}/^{39}\text{Ar}$ step-heating method. This approach yields two distinct sources of kinetic information (the age and Arrhenius spectra) from which quantitative measures of discrete Ar retentivity can be obtained. Provided a high correlation is observed between these two spectra, unique thermal history data can be obtained, regardless of choice of diffusion model.

With the advent of ion microprobe depth profiling, measurable gradients of Pb/Th and Pb/U have been observed over sub- μm length scales in accessory minerals. Ion microprobe depth profiling analysis is a highly underutilized method of thermochronologic analysis. Where Th-Pb gradients in monazite can be shown to be due

to diffusive Pb loss, they contain potentially valuable thermochronological. Although routine application of this approach using monazite is at present limited by uncertainty regarding extrapolation of kinetic models, the method has considerable promise for the future.

References

- Arnaud NO, Kelley SP (1995) Evidence for excess argon during high-pressure metamorphism in the Dora Maira Massif (western Alps, Italy) using a ultra-violet laser ablation ion microprobe ^{40}Ar - ^{39}Ar technique. *Contrib. Mineral. Petrol.* 121:1-11
- Arnaud NO, Kelley SP (1997) Argon behavior in gem quality orthoclase from Madagascar: Experiments and consequences for geochronology. *Geochim Cosmochim Acta* 61:3227-3255
- Axen GJ, Grove M, Stockli D, Lovera OM, Rothstein DA, Fletcher JM, Farley K, Abbott PL (2000) Thermal evolution of Monte Blanco Dome; low-angle normal faulting during Gulf of California rifting and late Eocene denudation of the eastern Peninsular Ranges. *Tectonics* 19:197-212
- Berger GW, York D (1981) Geothermometry from $^{40}\text{Ar}/^{39}\text{Ar}$ dating experiments. *Geochim Cosmochim Acta* 45:795-811
- Berger GW, York D, Dunlop DJ (1979) Calibration of Grenvillian palaeopoles by $^{40}\text{Ar}/^{39}\text{Ar}$ dating. *Nature* 277:46-48
- Cherniak DJ, Watson EB, Grove M, Harrison TM (2004) Pb diffusion in monazite: A combined RBS/SIMS study. *Geochim Cosmochim Acta* 68:829-840
- Compston W, Williams IS, Meyer C (1984) U-Pb geochronology of zircons from Lunar Breccia 73217 using a sensitive, high mass resolution ion microprobe. *Proceed 14th Lunar Planet Sci Conf Part 2. Jour Geophys Res* 89:8525-8534
- Copeland P, Harrison TM, Kidd WSF, Ronghua X, Yuquan Z (1987) Rapid early Miocene acceleration of uplift in the Gandese Belt, Xizang-southern Tibet, and its bearing on accommodation mechanisms of the India-Asia collision. *Earth Planet Sci Lett* 86:240-252
- Crank J (1975) *The Mathematics of Diffusion*, 2nd edition, Oxford University Press, London
- Dodson MH (1973) Closure temperature in cooling geochronological and petrological systems. *Contrib Mineral Petrol* 40:259-274
- Dodson MH (1986) Closure profiles in cooling systems. *In: Materials Science Forum*, Vol 7, Trans Tech Publications, Aedermannsdorf, Switzerland, p 145-153
- Foland KA (1974) ^{40}Ar diffusion in homogeneous orthoclase and an interpretation of Ar diffusion in K-feldspar. *Geochim Cosmochim Acta* 38:151-166
- Foland KA (1994) Argon diffusion in feldspars. *In Feldspars and their reactions* (ed. I. Parsons) pp. 415-447. Kluwer, Dordrecht
- Foster DA, Harrison, TM, Copeland PC, Heizler MT (1990) Effects of excess argon within large diffusion domains on K-feldspar age spectra. *Geochim Cosmochim Acta* 54:1699-1708
- Giletti BJ (1974) Studies in diffusion I: Argon in phlogopite mica. *In: Geochemical transport and kinetics*. AW Hofmann, BJ Giletti, HS Yoder Jr, RA Yund (eds) Carnegie Inst. Wash. Publ 634, p 107-115

- Girard JP, Onstott TC (1991) Application of $^{40}\text{Ar}/^{39}\text{Ar}$ laser probe and step-heating techniques to the dating of authigenic K-feldspar overgrowths. *Geochim Cosmochim Acta* 55:3777-3793
- Grove M (1993) Thermal histories of southern California basement terranes. PhD dissertation, University of California, Los Angeles, CA
- Grove M, Harrison TM (1996) ^{40}Ar diffusion in Fe-rich biotite. *Am Min* 81: 940-951
- Grove M, Harrison TM (1999) Monazite Th-Pb age depth profiling. *Geology* 27: 487-490
- Harrison TM, Zeitler PK (2005) Fundamentals of noble gas thermochronometry. *Rev Mineral Geochem* XX:YYY-YYY
- Harrison TM, Yin A, Grove M, Lovera OM, Ryerson FJ (2000) The Zedong Window: A record of superposed Tertiary convergence in southeastern Tibet. *Jour Geophys Res* 105:19211-19230
- Harrison TM, Grove M, Lovera OM, Catlos EJ, D'Andrea J (1999) The origin of Himalayan anatexis and inverted metamorphism: Models and constraints. *Jour Asian Earth Sci* 17:755-772
- Harrison TM, Grove M, Lovera OM, Catlos EJ (1998) A model for the origin of Himalayan anatexis and inverted metamorphism. *Jour Geophys Res* 103:27,017-27,032
- Harrison TM, Leloup PH, Ryerson FJ, Tapponnier P, Lacassin R, Chen W (1996) Diachronous initiation of transtension along the Ailao Shan-Red River Shear Zone, Yunnan and Vietnam. *In: The Tectonic Evolution of Asia*, Yin A, Harrison TM (eds), Cambridge Press, London, p 205-226
- Harrison TM, Copeland P, Kidd WSF, Lovera OM (1995) Activation of the Nyainqentanglha shear zone: implications for uplift of the southern Tibetan Plateau. *Tectonics* 14: 658-676
- Harrison TM, Duncan I, McDougall I (1985) Diffusion of ^{40}Ar in biotite: Temperature, pressure and compositional effects. *Geochim Cosmochim Acta* 49: 2461-2468
- Harrison TM, Armstrong RL, Naeser CW, Harakal JE (1979) Geochronology and thermal history of the Coast Plutonic Complex, near Prince Rupert, British Columbia. *Canadian J Earth Sci* 16: 400-410
- Hodges KV (1991) Pressure-temperature-time paths. *Ann Rev Earth Planet Sci* 19:207-236
- Hodges KV, Hames WE, Bowring SA, (1994) $^{40}\text{Ar}/^{39}\text{Ar}$ age gradients in micas from a high-temperature/low-pressure metamorphic terrain: Evidence for very slow-cooling and implications for the interpretation of age spectra *Geology* 22:55-58
- Kapp JLD, Harrison TM, Grove M, Lovera OM, Kapp PA, Lin D (2004) The Nyainqentanglha Shan: A window into the tectonic, thermal and geochemical evolution of the Lhasa block, southern Tibet. *J. Geophys Res* (in press)
- Kelley SP, Arnaud NO, Okay AI (1994) Anomalously old Ar-Ar ages in high pressure metamorphic terrains. *Min Mag* 58A:468-469
- Kelley SP, Wartho JA (2000) Rapid kimberlite ascent and the significance of Ar-Ar ages in xenolith phlogopites. *Science* 289:609-611
- Lee JKW, Onstoot TC, and Hames JA (1990) An $^{40}\text{Ar}/^{39}\text{Ar}$ investigation of the contact effects of a dyke intrusion, Kapuskasing Structural Zone, Ontario. A comparison of laser microprobe and furnace extraction techniques. *Contrib Mineral Petrol* 105:87-105

- Lovera OM, Heizler MT, Harrison TM (1993) Argon diffusion domains in K-feldspar II: kinetic properties of MH-10. *Contrib Mineral Petrol* 113:381-393
- Lovera OM, Grove M, Harrison TM (2002) Systematic analysis of K-feldspar $^{40}\text{Ar}/^{39}\text{Ar}$ step-heating experiments II: Relevance of laboratory K-feldspar argon diffusion properties to Nature. *Geochim Cosmochim Acta* 66:1237-1255
- Lovera OM, Grove M, Harrison TM, Mahon KI (1997) Systematic analysis of K-feldspar $^{40}\text{Ar}/^{39}\text{Ar}$ step-heating experiments I: Significance of activation energy determinations. *Geochim Cosmochim Acta* 61:3171-3192
- Lovera OM, Richter FM, Harrison TM (1989) $^{40}\text{Ar}/^{39}\text{Ar}$ geothermometry for slowly cooled samples having a distribution of diffusion domain sizes. *Jour Geophys Res* 94: 17917-17935
- Lovera OM, Richter FM, Harrison TM (1991) Diffusion domains determined by ^{39}Ar release during step heating. *Jour Geophys Res* 96:2057-2069
- Mattinson JM (1978) Age, origin, and thermal histories of some plutonic rocks from Salinian Block of California. *Contrib Mineral Petrol* 67:233-245
- McDougall I, Harrison TM (1999) *Geochronology and thermochronology by the $^{40}\text{Ar}/^{39}\text{Ar}$ Method*. 2nd ed., Oxford University Press, New York
- Mojzsis SJ, Harrison TM (2002) Establishment of a 3.83-Ga magmatic age for the Akilia tonalite (southern West Greenland). *Earth Planet Sci Lett* 202:563-576
- Hames, WE, Cheney, JT (1997) On the loss of ^{40}Ar from muscovite during polymetamorphism. *Geochim Cosmochim Acta* 61:3863-3872
- Onstott TC, Phillips D, Pringle-Goodell L (1991) Laser microprobe measurement of chlorine and argon zonation in biotite. *Chem Geol* 90:145-168
- Parsons I, Brown W L, Smith JV (1999) $^{40}\text{Ar}/^{39}\text{Ar}$ thermochronology using alkali feldspars; real thermal history or mathematical mirage of microtexture? *Contrib Mineral Petrol* 136:92-110
- Pickles CS, Kelley SP, Reddy SM, Wheeler J (1997) Determination of high spatial resolution argon isotope variations in metamorphic biotites. *Geochim Cosmochim Acta* 61:3809-3833
- Press WH, Flannery BP, Peukolsky SA, Vetterling WT (1998) *Numerical Recipes: The Art of Scientific Computing*. Cambridge University Press, New York
- Price WL (1977) A controlled random search procedure for global optimization. *Computer Jour* 20:367-370
- Purdy JW, Jäger E (1976) K-Ar ages on rock-forming minerals from the Central Alps. *Mem 1st Geol Min Univ Padova* 30, 31 pp
- Quidelleur X, Grove M, Lovera OM, Harrison TM, Yin A, Ryerson FJ (1997) The thermal evolution and slip history of the Renbu Zedong Thrust, southeastern Tibet. *Jour Geophys Res* 102:2659-2679
- Reddy SM, Kelley SP, and Wheeler J (1996) A $^{40}\text{Ar}/^{39}\text{Ar}$ laser probe study of micas from the Sesia Zone, Italian Alps: implications for metamorphic and deformation histories. *J Metamorphic Geol* 14:493-508.
- Richter FM, Lovera OM, Richter FM, Copeland P (1991) Tibetan tectonics from a single feldspar sample: An application of the $^{40}\text{Ar}/^{39}\text{Ar}$ method. *Earth Planet Sci Lett* 105:266-276

- Scaillet S, Féraud G, Lagabrielle Y, Ballèvre M, Ruffet G (1990) $^{40}\text{Ar}/^{39}\text{Ar}$ laser probe dating by step heating and spot fusion of phengites from the Dora Maira nappe of the western Alps, Italy. *Geology* 18:741-744
- Sherlock S, Kelley S, Inger S, Harris N, Okay A (1999) ^{40}Ar - ^{39}Ar and Rb-Sr geochronology of high-pressure metamorphism and exhumation history of the Tavsanli Zone, NW Turkey. *Contrib Mineral Petrol* 137:46-58
- Hames WE, Andresen A (1996) Timing of Paleozoic orogeny and extension in the continental shelf of north-central Norway as indicated by laser $^{40}\text{Ar}/^{39}\text{Ar}$ muscovite dating. *Geology* 24:1005-1008
- Warnock AC, van de Kamp PC (1999) Hump-shaped $^{40}\text{Ar}/^{39}\text{Ar}$ age spectra in K-feldspar and evidence for Cretaceous authigenesis in the Fountain Formation near Eldorado Springs, Colorado. *Earth Planet Sci Lett* 174:99-111
- Wartho J, Kelley, SP (2003) $^{40}\text{Ar}/^{39}\text{Ar}$ ages in mantle xenolith phlogopites: determining the ages of multiple lithospheric mantle events and diatreme ascent rates in Southern Africa and Malaita, Solomon Islands. *Geol Soc Spec Pub* 220:231-248
- Wartho J, Kelley SP, Brooker RA, Carroll MR, Villa IM, Lee MR (1999) Direct measurement of Ar diffusion profiles in a gem-quality Madagascar K-feldspar using the ultra-violet laser ablation microprobe (UVLAMP). *Earth Planet Sci Lett* 170:141-153
- Willett SD (1997) Inverse modeling of annealing of fission tracks in apatite; 1, A controlled random search method. *Am J Sci* 297:939-969
- Zeitler PK, Fitz Gerald JD (1986). Saddle-shaped $^{40}\text{Ar}/^{39}\text{Ar}$ age spectra from young, microstructurally complex potassium feldspars. *Geochim Cosmochim Acta* 50:1185-1199
- Zeitler PK (1993) Inversion of $^{40}\text{Ar}/^{39}\text{Ar}$ age spectra using the controlled-random-search method. *EOS* 74:650
- Zeitler PK (2004) Arvert 4.0.1. Inversion of $^{40}\text{Ar}/^{39}\text{Ar}$ age spectra. User's Manual (<http://www.ees.lehigh.edu/EESdocs/geochron/downloads/arvert401guide-US.pdf>).

Figure captions

Figure 1. Schematic thermal history (solid curve) showing initial slow cooling, followed by a rapid cooling segment, and then a second slow cooling phase. Crosses in (a) represent three thermochronometers with varying T_c . Note that uncertainties in T_c permit a wide range of possible thermal history interpretations, including the linear path shown by the dashed line. (b) shows a continuous thermal history obtained by knowing the concentration distribution of the daughter product.

Figure 2. Typical K-feldspar age and Arrhenius properties. (a) Age spectrum (left axis) and $\log(r/r_o)$ spectrum (right axis) for N13 K-feldspar (Harrison et al. 2000). Note correlated behavior, particular over the interval of gas release between the disappearance of low-temperature Cl-correlated $^{40}\text{Ar}_E$ and the onset of melting above 1100°C . C_{fg} refers to correlation coefficient calculated by Lovera et al. (2002). (b) Arrhenius plot showing measured diffusivities, reference Arrhenius law (ρ_o) defined by initial gas release (see text), and sample calculation of $\log(r/r_o)$ value at 1000°C (see text).

Figure 3. Variability of K-feldspar age spectra in nature. (a) Well-behaved monotonically increasing K-feldspar age spectra after correction for Cl-correlated excess ^{40}Ar ($^{40}\text{Ar}_E$) from the Renbu Zedong thrust (Quidelleur et al. 1997). (b) K-feldspar age spectra heavily contaminated with both low- and high-temperature $^{40}\text{Ar}_E$. Note U-shaped age spectra with least affected gas release at 15-35 cumulative % $^{39}\text{Ar}_K$ release. (c) K-feldspar age spectra exhibiting intermediate age maxima (IAM). These are smoothly continuous and are characteristically developed over the 15-35 cumulative % $^{39}\text{Ar}_K$ interval of gas release where $^{40}\text{Ar}_E$ contamination tends to be minimal. (d) Survey of more than 200 K-feldspars from Lovera et al. (2002) indicating proportions of “well-behaved” samples, samples exhibiting high-temperature $^{40}\text{Ar}_E$ contamination, and samples with IAM.

Figure 4. Application of the multi diffusion domain (MDD) model to recover crustal thermal histories from K-feldspar. After calibrating the MDD model with the diffusion properties of the samples, the thermal history is forward modeled by fitting the age spectrum. (a) MDD fit to measured Arrhenius data. Domain structure is indicated schematically by grey line. Thickness is proportional to concentration. (b) Input thermal history corresponding to calculated age spectrum (below). Solid line indicates portion of temperature-time path relevant to sample. (c) Calculated MDD age spectrum.

Figure 5. Top: a-d, CRS convergence sequence for simulated multidomain K-feldspar cooling at $10^\circ\text{C}/\text{m.y.}$, Monte Carlo, 200, 1000, and 4886 iterations. Middle, e and f, predicted age spectra at start and end of model. Bottom: summary of final results after convergence. Box shows time span where age spectrum has constraining power.

Figure 6. Summary of CRS model for multidomain K-feldspar having a more complex non-linear cooling history. Boxes shows time span where age spectrum has constraining power, and time where U-Th/He apatite age provides a constraint.

Figure 7. Application of the variational approach to MDD analysis of 96MX-001 K-feldspar (Axen et al. 2000). (a) Measured age spectrum and 50 best-fit MDD age spectra calculated from ten equivalent MDD domain distributions with activation energy (E) values defining a normal distribution about the measured activation energy for the sample (53 ± 2 kcal/mol). See text and Lovera et al. (2002) for additional details. (b) Set of 50 thermal histories corresponding to best-fit age spectra. Note that $\pm 17^\circ\text{C}$ variation in temperature-time histories results from propagation of ± 2 kcal/mol error in E . (c) Confidence intervals (90%) for the overall distribution and median of the 50 thermal histories. Note that median shows only portion of thermal history constrained by age data from the sample. Additional thermochronologic constraints for 96MX-001 from Axen et al. (2000) are shown for reference.

Figure 8. (A) Comparison of variational and controlled-random search (CRS) analyses of 96MX-001 K-feldspar (Axen et al. 2000). (B) CRS model results are composite of 200 best-fit thermal histories calculated from two different starting pools of random thermal histories (shown in (C) and (D) respectively). CRS models based on single domain distribution having same activation energy as the mean of used in variational models (53 kcal/mol).

Figure 9. Results of numerical simulation of domain instability during slow-cooling from Lovera et al. (2002). An domain structure is instantly converted to less retentive domain structure by forming small domains from pre-existing larger domains at temperatures between $150\text{-}300^\circ\text{C}$. All runs have the same imposed linearly decreasing thermal history. See text and Lovera et al. (2002) for additional details. (a) Age spectra for original high-temperature domain distribution and transformed samples. Note formation of intermediate age maxima for transformations taking place at 200°C or lower. (b) calculated thermal histories for $150\text{-}300^\circ\text{C}$ model runs. Note that there is essentially no impact at or above 250°C for the conditions explored in these calculations. At 200°C and below, calculated thermal histories and progressively nonsensical.

Figure 10. (a) Th-Pb age profile in the near surface region of monazite DH-68-96 (Grove and Harrison 1999). The curve fit to the data reflects the diffusion calibration described in the text and thermal history shown in (b), the thermal history required to fit the Th-Pb age gradient. Hatched region shows the T - t region that are consistent with the thermochronometric and thermobarometric data and other geologic constraints.

Table 1. Closure function $4S_2(x)$

x	<i>Plane sheet</i>	<i>Cylinder</i>	<i>Sphere</i>
0.00	0.41194	1.02439	1.38629
0.05	0.41653	1.03831	1.38980
0.10	0.43036	1.03990	1.40039
0.15	0.45367	1.05944	1.41826
0.20	0.48685	1.08728	1.44371
0.25	0.53047	1.12393	1.47723
0.30	0.58535	1.17011	1.51946
0.35	0.65254	1.22676	1.57131
0.40	0.73347	1.29515	1.63392
0.45	0.82999	1.37695	1.70887
0.50	0.94458	1.47439	1.79824
0.55	1.08057	1.59051	1.90484
0.60	1.24254	1.72949	2.03262
0.65	1.43699	1.89732	2.18721
0.70	1.67352	2.10291	2.37704
0.75	1.96710	2.36026	2.61543
0.80	2.34291	2.69317	2.92511
0.85	2.84826	3.14674	3.34950
0.90	3.58951	3.82350	3.98796
0.95	4.90636	5.05471	5.16455
0.96	5.33878	5.46577	5.56120
0.97	5.90027	6.00366	6.08275
0.98	6.69734	6.77401	6.83402
0.99	8.06977	8.11483	8.16128
0.995	9.44913	9.47507	9.49661
Volume average	1.58611	2.71862	3.43012

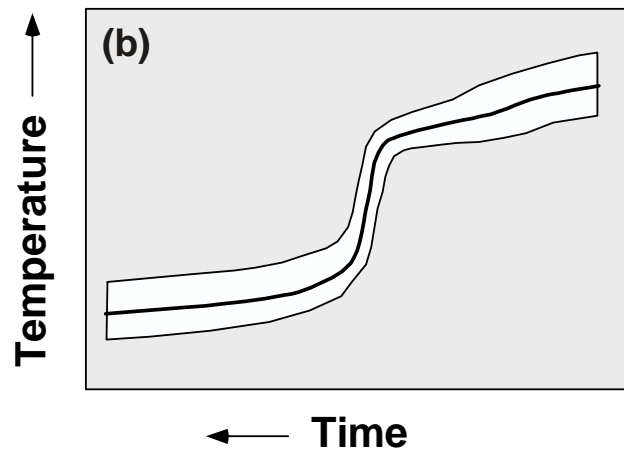
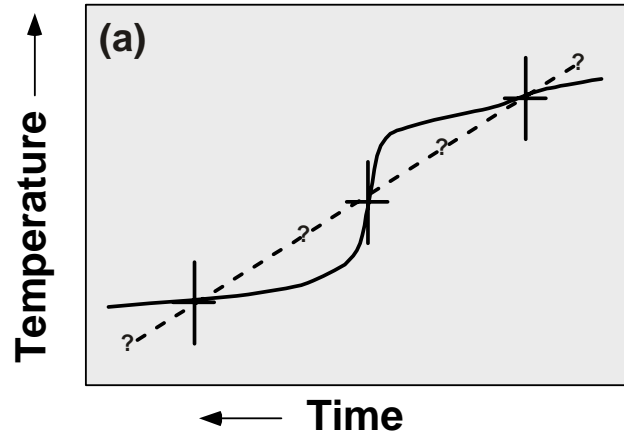


Figure 1

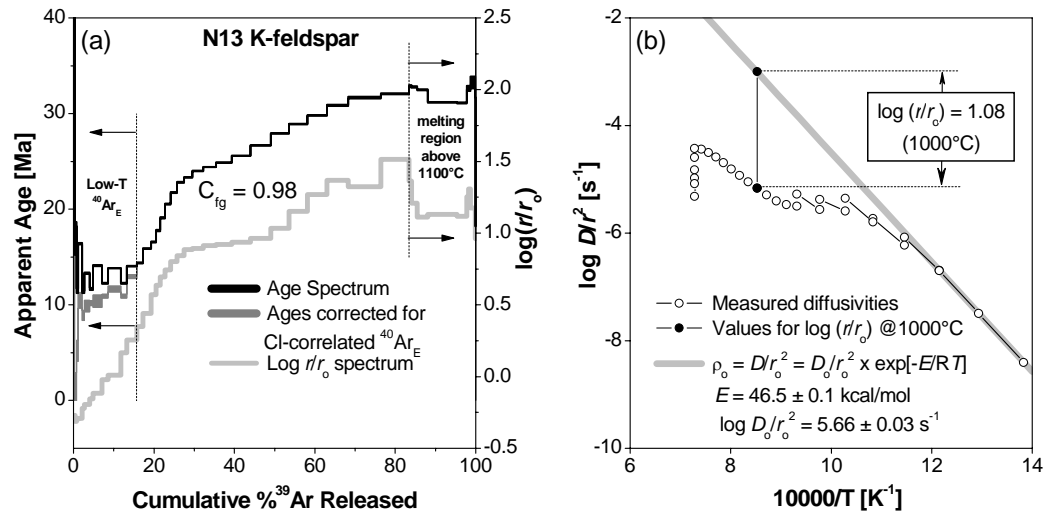


Figure 2

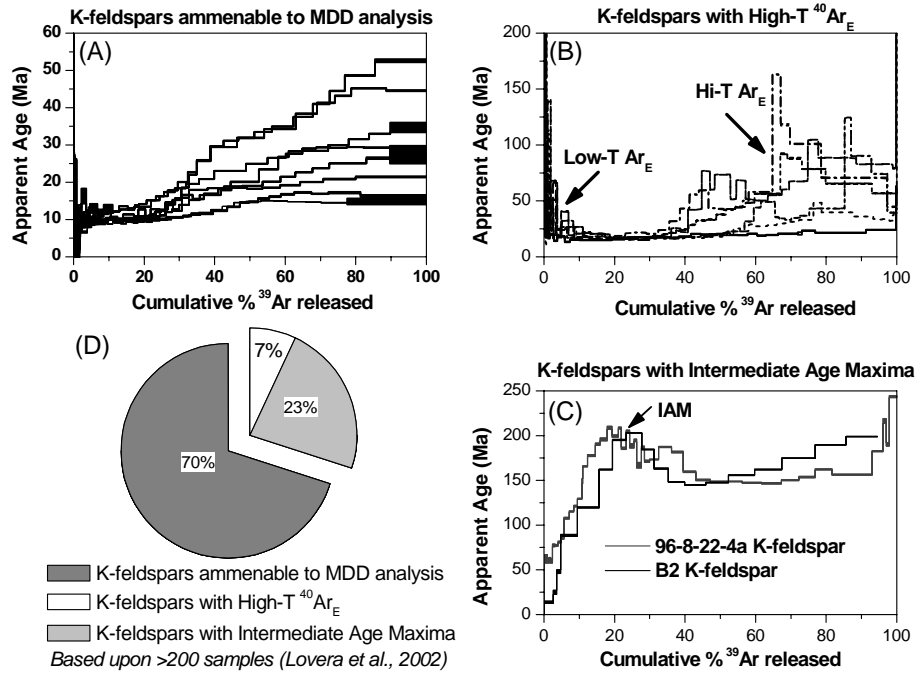


Figure 3

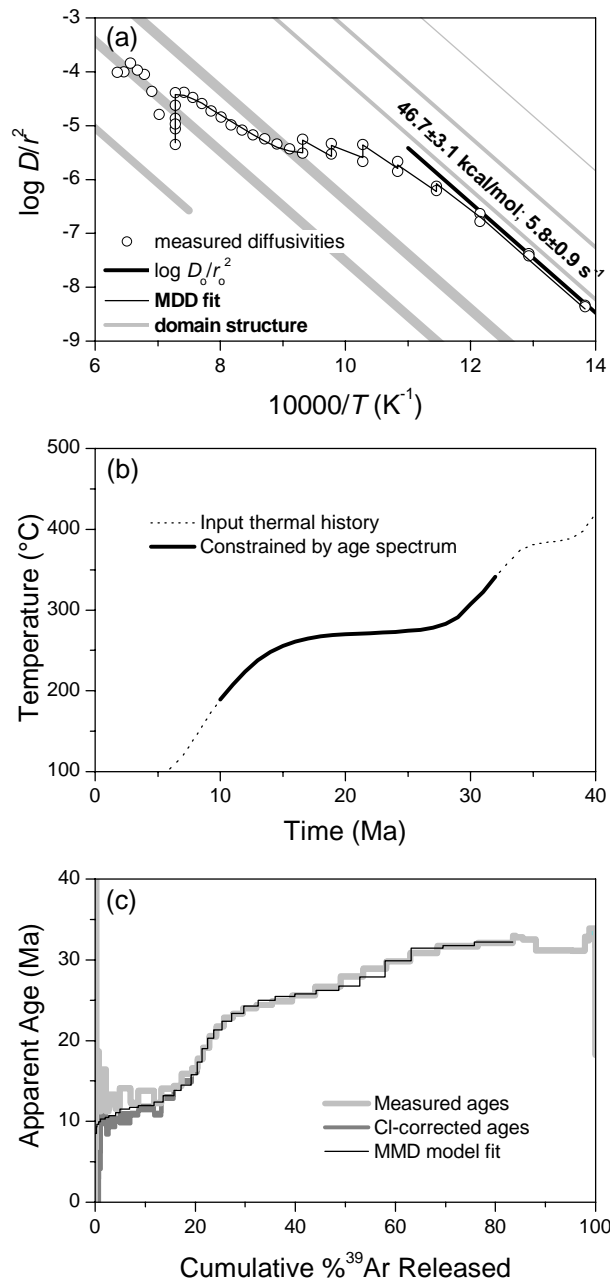


Figure 4

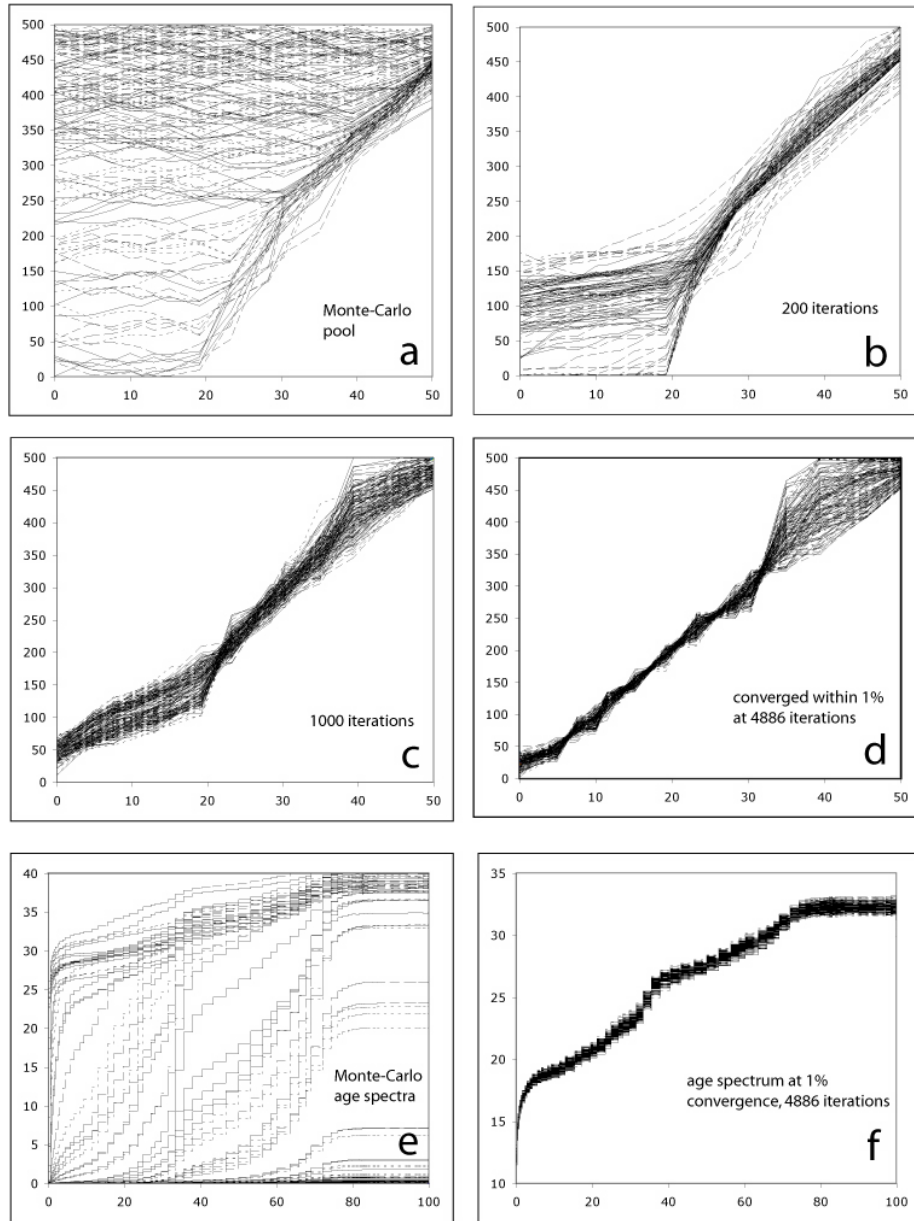


Figure 5

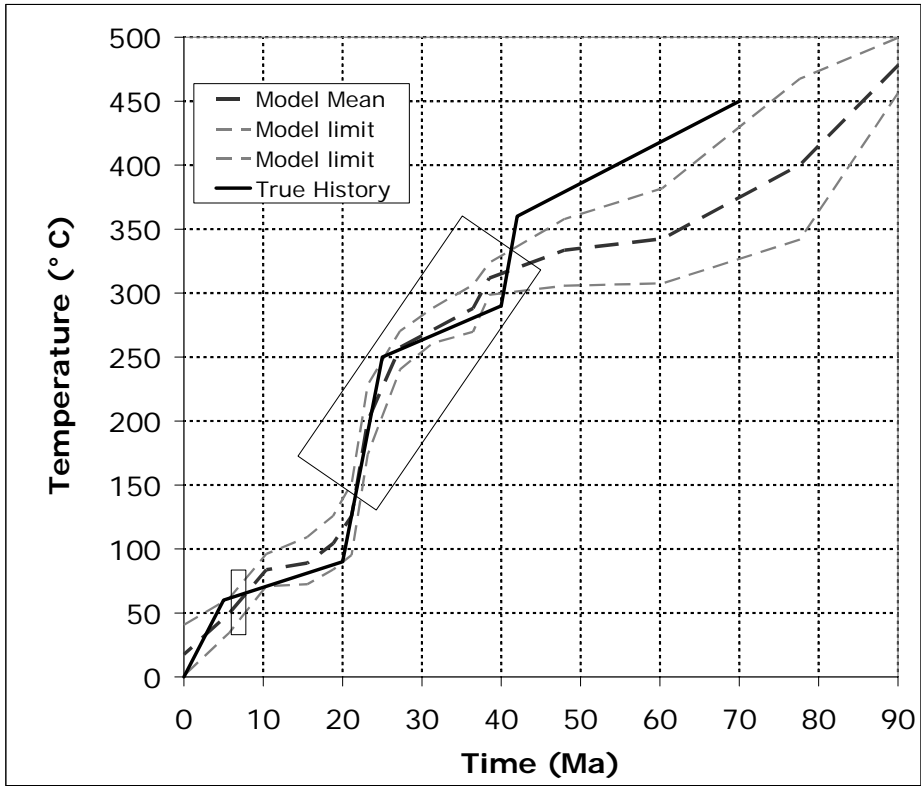


Figure 6

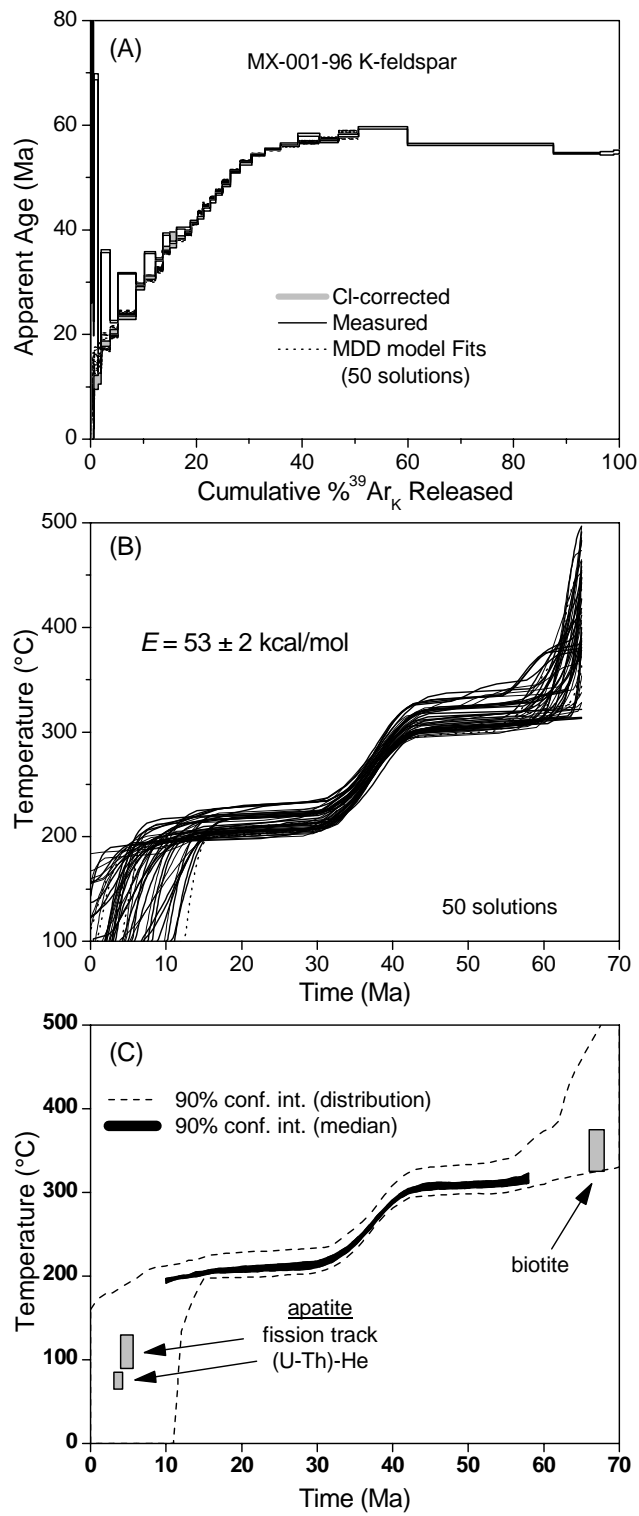


Figure 7

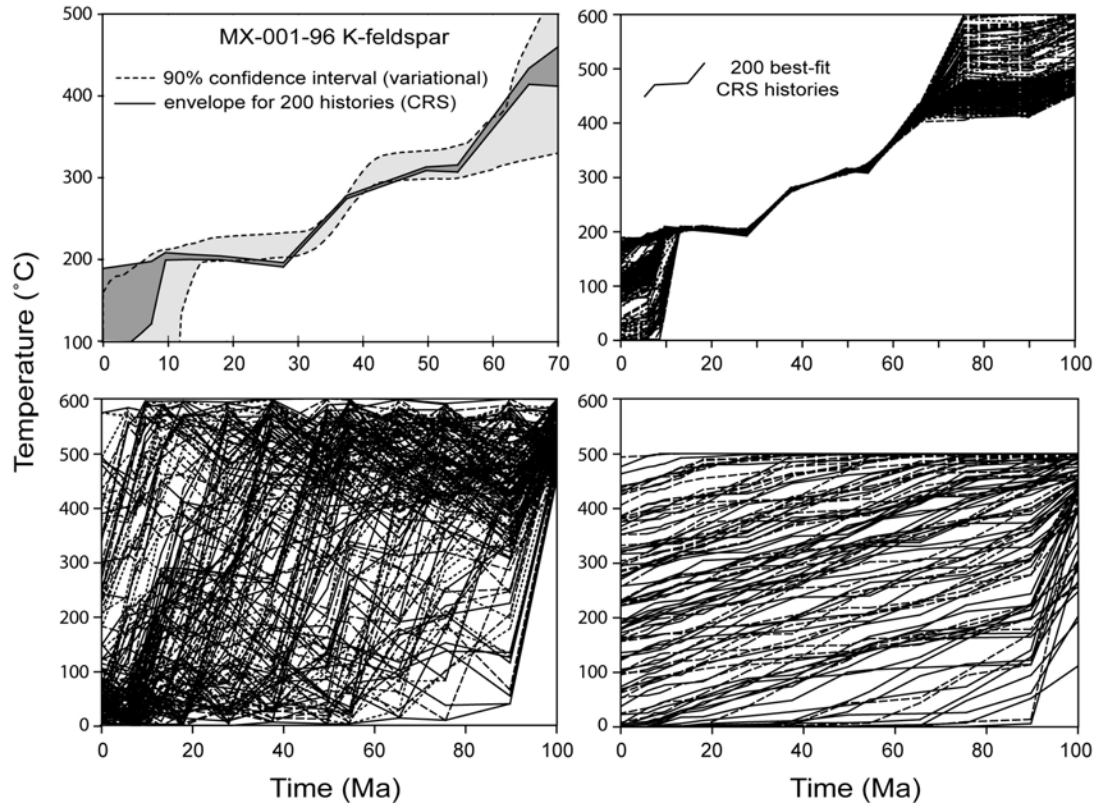


Figure 8

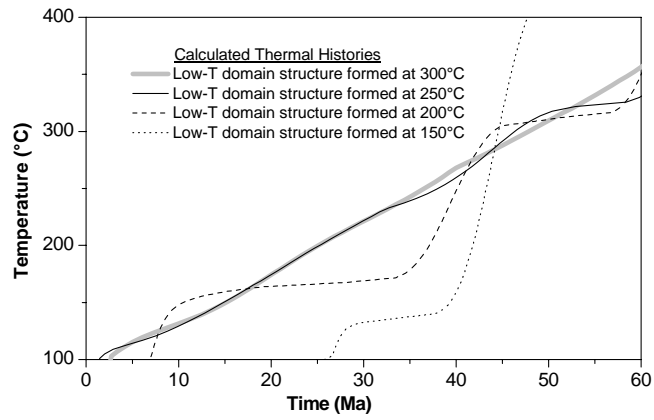
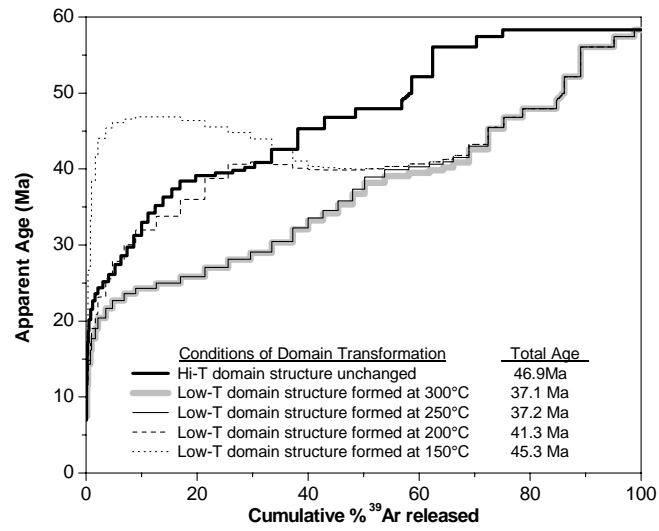


Figure 9

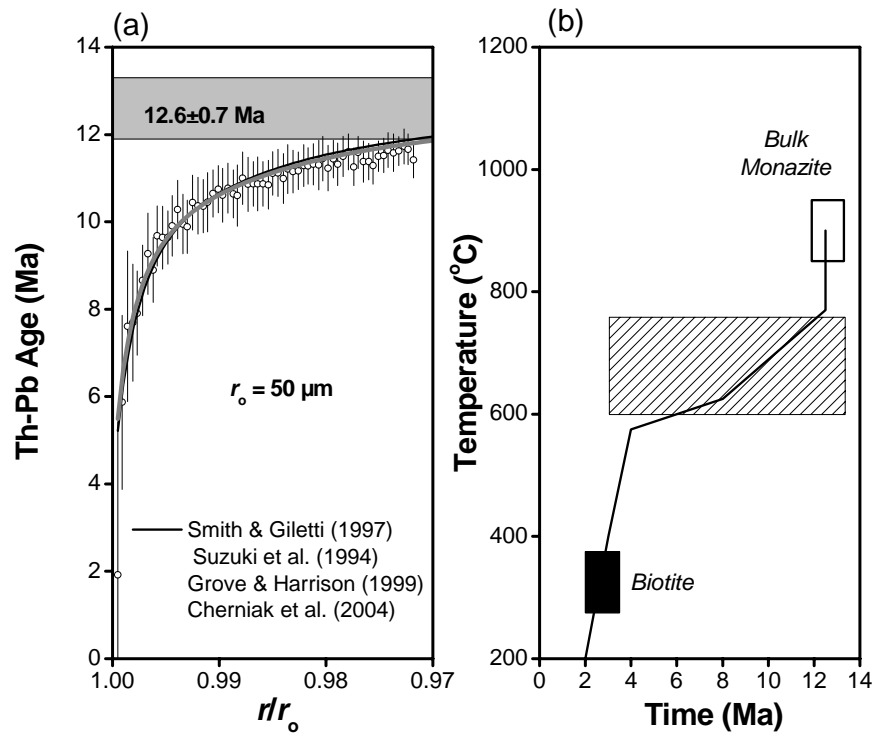


Figure 10